Increased illumination uniformity and reduced photodamage offered by the Lissajous scanning in fiber-optic two-photon endomicroscopy

Wenxuan Liang
Kartikeya Murari
Yuying Zhang
Yongping Chen
Ming-Jun Li
Xingde Li

Increased illumination uniformity and reduced photodamage offered by the Lissajous scanning in fiber-optic two-photon endomicroscopy

Wenxuan Liang,[a] Kartikeya Murari,[a] Yuying Zhang,[a] Yongping Chen,[a] Ming-Jun Li,[b] and Xingde Li[a]

[a]Johns Hopkins University, Department of Biomedical Engineering, Baltimore, Maryland 21205
[b]Science and Technology Division, Corning Incorporated, SP-AR-02-2, Corning, New York 14831

Abstract. We compare the illumination uniformity and the associated effects of the spiral and Lissajous scanning patterns that are commonly used in an endomicroscope. Theoretical analyses and numerical simulations were first performed to quantitatively investigate the area illumination density in the spiral scanning pattern. The results revealed the potential problem of manifest photodamage due to the very high illumination density in the center of the spiral scan. Similar analyses of the Lissajous scanning pattern, which can be conveniently implemented on the same endomicroscope with no hardware modifications, showed a more uniform illumination density with about an 80-fold reduction in the peak illumination density. To underscore the benefit offered by the improved illumination uniformity, we conducted *in vitro* two-photon fluorescence imaging of cultured cells stained with a LIVE/DEAD viability assay using our home-built, fiber-optic, two-channel endomicroscopy system. Both the spiral and the Lissajous scans were implemented. Our experimental results showed that cells near the spiral scan center experienced obvious photodamage, whereas cells remained alive over the entire region under the Lissajous beam scanning, confirming the predicted advantage offered by the Lissajous scan over this spiral scan in an endomicroscopy setting.
© 2012 Society of Photo-Optical Instrumentation Engineers (SPIE). [DOI: 10.1117/1.JBO.17.2.021108]

Keywords: endomicroscopy; two-photon fluorescence; scanning probe.

Paper 11537SS received Sep. 22, 2011; revised manuscript received Jan. 3, 2012; accepted for publication Jan. 9, 2012; published online Feb. 27, 2012.

1 Introduction

Two-photon fluorescence (TPF) is a powerful technique for three-dimensional depth-resolved microscopic imaging[1]. Its quadratic dependence on the intensity of incident light ensures the localization of the two-photon excitation within the tightly focused volume and provides TPF with intrinsic optical sectioning ability with reduced out-of-focus photodamage. To translate this useful imaging modality to broader applications, particularly for *in vivo* and clinical imaging of internal organs, extensive efforts have been made to develop a miniature TPF microscope and ultimately a flexible fiber-optic TPF endomicroscope.[2–7] One solution to realize stable two-dimensional *en face* beam scanning in a miniaturized endomicroscope probe is to pass a double-clad fiber (DCF) through a compact tubular piezoelectric (PZT) actuator (e.g., a diameter of 1.2–1.5 mm) and glue the fiber to the end of the PZT tube as shown in Fig. 1 (Refs. 6,8,9). The outer surface of the PZT tube is divided symmetrically into four quadrants forming two orthogonal pairs of driving electrodes. Appropriately designed voltage waveforms can be applied to electrodes to drive the PZT tube, which actuates the fiber cantilever into a desired scanning pattern. The scanning fiber cantilever tip is imaged onto the sample by a miniature objective lens to perform beam scanning.

Conventionally, amplitude-modulated sine and cosine waveforms with the frequency fixed at or close to the mechanical resonant frequency of the fiber cantilever are applied to the two pairs of electrodes to produce an open-close spiral scanning pattern. Though robust and amenable to easy position calibration, such a spiral pattern inevitably results in a much higher area illumination density of the excitation light in the center of the scanned region than in the periphery and may consequently lead to photodamage in the center region, prohibiting longitudinal imaging of the sample.

One intuitive solution to this problem is to modulate the laser power according to the scanning position, which can be achieved by using an acousto-optic modulator to appropriately attenuate the excitation light when scanning the central region. Another is to modify the scan pattern to other patterns, such as the Lissajous scan. Lissajous scanning has been used in miniaturized TPF microscopes, either by stiffening the fiber on one side to create two different vibration resonance frequencies in the two lateral directions[2,3] or through two-dimensional asynchronous scanning of a microelectromechanical system (MEMS) mirror.[10,11] Our implementation of the Lissajous beam scanning reported in this paper, however, was realized by using the ultracompact fiber-optic resonant scanner shown in Fig. 1, which is conventionally operated in the spiral scanning mode. Lissajous scanning was achieved by simply choosing slightly different driving frequencies (but still close to the mechanical resonant frequency of the fiber cantilever) for the two pairs of electrodes.

In this report, theoretical analyses and numerical simulations were first performed to compare the distribution of area illumination density in both scanning patterns, which revealed the feasibility of the Lissajous scan to achieve more uniform

Address all correspondence to: Xingde Li, RM 731B, Ross Building, 720 Rutland Avenue, Baltimore. Tel: 410-955-0075; Fax: 410-502-9814; E-mail: xingde@jhu.edu
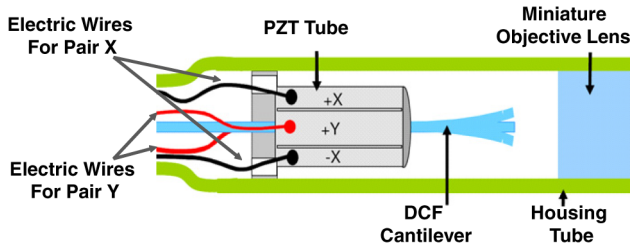
Fig. 1 Schematic of the distal end of a fiber-optic scanning nonlinear optical endomicroscope probe. The piezoelectric (PZT) tube, the double-clad fiber (DCF) cantilever, and the miniature objective lens were encased in a hypodermic housing tube with an overall outer diameter of 2.4 mm. The two pairs of electrodes on the PZT tube surface are marked X and Y, with the corresponding electric wires colored black and red, respectively.

illumination over the entire scanned region compared with the traditional spiral scan. *In vitro* cell viability experiments were conducted using our home-built, fiber-optic endomicroscope, and the results confirmed the reduced photodamage offered by the Lissajous scanning pattern. To the best of our knowledge, this is the first time such systematic analyses and comparison of these two scanning patterns for fiber-optic TPF endomicroscope have been reported in literature.

2 Theoretical Analysis and Numerical Simulation

The driving mechanism of spiral scanning is detailed in our previous reports.[4,8,9] Ideally, the spiral scanning path of the fiber tip can be described in polar coordinates as follows:

$$r = \frac{A}{2} \cdot [1 - \cos(2\pi f_S t)], \qquad \theta = 2\pi f_R t. \qquad (1)$$

Here, frequency f_R, selected to be close to the mechanical resonant frequency of the fiber cantilever, represents the circumferential scanning frequency of the fiber tip, and f_S and A are the modulation frequency and amplitude of the PZT drive waveform, respectively. An example of an ideal spiral scanning path is shown in Fig. 2(a), where $f_S = 1$ Hz and $f_R = 100$ Hz. (These values are for illustrative purposes only. Practically, $f_S \sim 1.336$ Hz and $f_R \sim 1.368$ kHz were used in our endomicroscope.) Because the circumferential scanning frequency is constant, the beam dwell time per unit length along the circumferential direction is longer in the central region, leading to a higher area illumination density. In addition, the beam-scanning speed along the radial direction (i.e., $r' = dr/dt$) is also nonuniform, as indicated by Eq. (1). The radial speed is faster over the ring-shape region with a radius about half the maximum scan radius and slower near the center and the periphery. Although this nonuniform radial speed is not the dominant factor causing the nonuniform illumination in the scan center, it does contribute to visibly higher area illumination density along the periphery as shown in Fig. 2.

Quantitatively, during an infinitesimal period δt, the area element illuminated by the fiber tip can be written in polar coordinates as $r \cdot \delta r \cdot \delta \theta$, which is proportional to $r \cdot r'$, the product of radius and the speed along the radial direction, whereas $\delta \theta \sim f_R \delta t$ remains constant for a constant circumferential scanning frequency f_R. With a constant light intensity emitted from the fiber tip, the area illumination density is thus inversely proportional to the product $r \cdot r'$. When the scanning fiber approaches
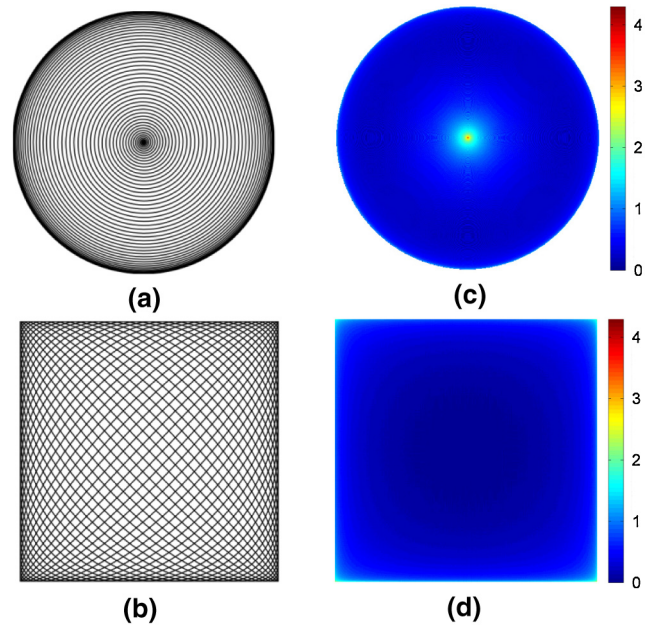
Fig. 2 Comparison of the spiral and Lissajous scanning patterns. Example scanning paths were drawn for (a) spiral and (b) Lissajous scanning patterns. Area illumination density is shown for (c) spiral and (d) Lissajous scanning, respectively. The color bar indicates the $\log_{10}$ value of the density level normalized by the minimal area illumination intensity of the entire scanned region. Note that low-frequency values ($f_S = 1$ and $f_R = 100$ for (a), $f_X = 31$ and $f_Y = 30$ for (b)) were adopted solely for illustrating the trajectories in (a) and (b), whereas practical frequency values ($f_S = 1.336$ and $f_R = 1,368$ for (c), $f_X = 1,368$ and $f_Y = 1,370$ for (d)) were used for simulating the area illumination density in (c) and (d).

the center, radius r and its derivative are both extremely small, thus resulting in a strikingly high illumination peak in the center. When fiber scans toward the periphery, only r' is diminishing, so the power density, though it grows relatively higher, is still much lower than near the center.

In the Lissajous scanning, the frequencies of the two PZT driving waveforms are slightly different, with the ideal scanning paths expressed in the Cartesian coordinates as follows:

$$x = A \cdot \sin(2\pi f_X \cdot t), \qquad y = A \cdot \sin(2\pi f_Y \cdot t). \qquad (2)$$

It is well-known that the Lissajous pattern repeats itself if and only if the ratio of the two frequencies is a rational number.[12] This requirement can be easily satisfied in practice by precisely controlling the driving waveforms. The overall repetition period is the least common multiple of the two repetition periods. Usually, only a slight difference is introduced between f_X and f_Y, so that scanning in each direction is repeated enough times before the whole pattern repeats itself, producing dense coverage of the scanned region. Figure 2(b) shows an example of a Lissajous scanning path with the ratio $f_X/f_Y = 30/31$. (Again, this ratio is simply illustrative. A 730/731 ratio was used in our endomicroscope.)

For the Lissajous scanning, the traces cross each other multiple times, making it very complicated to derive a closed-form analytical expression for the area illumination density. However, qualitative analysis can be performed intuitively. In contrast to the spiral scanning, the fiber is not confined to a small region during the Lissajous scanning, thus the area illumination density

at any given point is roughly inversely proportional to the instantaneous speed of the fiber tip. From the ideal trajectory given by Eq. (2), the fiber tip moves fastest in the center and slows down when it approaches the edges of the scanned region, with its speed in either the x- or y-direction reducing to zero at the edge. Thus the area illumination density is expected to remain low in the central region, increase near the edges, and become highest in the four corners.

Numerical simulation was performed to verify our theoretical analysis and quantitatively compare the area illumination density of the two scanning patterns. For the spiral scanning, we set the modulation amplitude $A = 1$, modulation frequency $f_S = 1.336$ Hz, and circumferential frequency $f_R = 1.368$ kHz. For the Lissajous scanning, we set the amplitude $A = 1$ and frequencies f_X and f_Y to be 1.368 kHz and 1.370 kHz, respectively. All these frequencies were chosen to be close to the frequencies used in practical imaging as detailed in next section. In both cases, a square region was discretized into 500×500 small identical square area elements. The dwell time of the fiber tip in each area element was used to represent the illumination distribution. The Cartesian position of the fiber tip was calculated at 25-ns increments according to Eq. (1) or Eq. (2), and the total number of time steps that the fiber tip spent in a given area element was found. After one complete scanning period (~ 0.37 and ~ 0.53 sec for the spiral and Lissajous scanning, respectively), the dwell time in each element was normalized by dividing the minimum value in the scanned region. (For the spiral scanning, those area elements outside the circular scanned region had zero dwell time and were ignored in analysis.) The results are plotted on a log scale and shown in Fig. 2(c) for the spiral and Fig. 2(d) for the Lissajous scanning, respectively.

It can be seen that the results from numerical simulations match our qualitative analysis above. The peak in the center of the spiral scanned region is about 4.3 orders of magnitude above the minimum. The density also arises near the periphery, but to a much lower extent (about 1 order of magnitude). For the Lissajous scanning, as predicted, the illumination density only rises when the fiber tip is very close to the edges and corners. The peak at the corners is about 2.4 orders of magnitude above the minimum, representing about an 80-fold improvement in the normalized magnitude over the spiral scanning. The reason for this reduction in the peak value is that during the Lissajous scanning, though the fiber tip nearly comes to a halt when it arrives at a corner, it does not linger in any small neighborhood for long as it does near the center of the spiral scanned region. Thus, not only the speed of the scanning fiber tip but also the area covered by the tip affect the final area illumination density.

3 Experimental Design and System Implementation

To verify the above theoretical analysis, we designed controlled *in vitro* experiments to evaluate and compare cell viability during the spiral and the Lissajous scanning. TPF imaging of cultured A431 squamous carcinoma cells was performed using a scanning fiber-optic endomicroscope under both the spiral and the Lissajous scanning. The selected indicator of cellular viability was the widely used LIVE/DEAD sperm viability kit (Invitrogen), which comprises two fluorescent dyes, SYBR-14 and propidium iodide (PI), both fluorescing only when bound to DNA.[13,14] Because SYBR-14 can penetrate intact cell membranes while PI cannot, live cells (with intact membranes) are labeled only by SYBR-14, which fluoresces

in the green wavelength range centered around 520 nm, whereas dead cells with ruptured membranes are labeled by PI, which fluoresces in the red region centered around 620 nm (in addition to being labeled by SYBR-14). The two-photon excitation wavelength in our experiment was set to 810 nm.[14] A431 cells used in our experiments were first incubated with the two dyes following the product protocol.[15] Considering that the working distance of the objective lens in our probe is about 200 μm in water, the cells were cultured directly on No. 0 coverslips with a thickness ~ 100 μm. Before being placed under the fiber-optic scanning endomicroscope, the coverslip was flipped upside down with the cells on the lower surface submerged in a solution containing both SYBR-14 and PI, and the top surface of the coverslip remained free of the dye solution.

When a cell dies from photodamage and its membrane ruptures, PI will enter the cell and bind to the DNA. Consequently, the fluorescence from the cell will turn from green (SYBR-14) to red (PI). To monitor and capture the two different fluorescence colors simultaneously, we implemented a dual-channel detection scheme on our home-built, fiber-optic endomicroscope system,[6] the schematic of which is shown in Fig. 3.

A tunable Ti:Sapphire laser (Chameleon Vision II; Coherent Inc., Santa Clara, CA) with built-in dispersion compensation served as the TPF excitation light source. A pair of parallel gratings (not shown in Fig. 3) outside the laser further prechirped the laser pulse to provide adequate dispersion compensation before the pulse was coupled into the core of a customized DCF used in the endomicroscope. The DCF had a single-mode core of a diameter ~ 4.2 μm and a large inner cladding of a diameter ~ 185 μm. In our experiments, the laser power delivered to the sample was set to ~ 60 mW, which was sufficient to induce photodamage within a short period (i.e., about a few minutes). The TPF signals collected by the same DCF (through the core and inner clad) were separated from excitation light by the first dichroic mirror (DM1 at 665 nm). The two fluorescence bands from the two dyes (SYBR-14 and PI) were further separated using a second dichroic mirror (DM2 at 580 nm) and detected by two photomultiplier tubes (PMT1 and PMT2). In the front of each PMT, two optical filters were used, with one short-pass filter blocking the residual excitation light and one band-pass
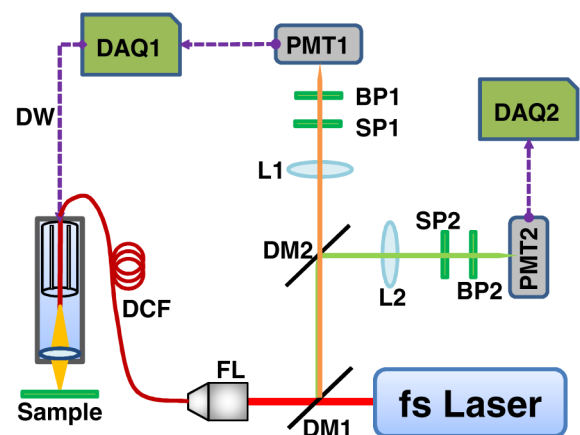
Fig. 3 Schematic of a dual-channel fiber-optic scanning TPF endomicroscope imaging system. The prechirping component is not shown here. Dashed arrows denote the flow of electrical signals. BP1 and BP2: Band-pass filters. DAQ1 and DAQ2: Data acquisition cards. DCF: Double-clad fiber. DM1 and DM2: Dichroic mirrors. DW: Driving waveform. FL: Fiber launcher. L1 and L2: Focusing lenses. PMT1 and PMT2: Photomultiplier tubes. SP1 and SP2: Short-pass filters.

filter appropriate for passing the desired fluorescence light (617 to 691 nm for PI and 510 to 560 nm for SYBR-14).
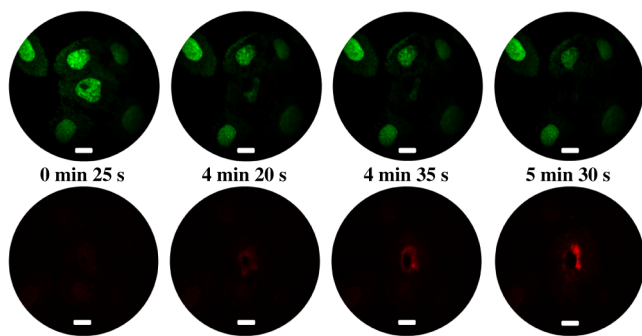
The photo current from each PMT was amplified, converted to voltage, and then digitized by two separate data acquisition (DAQ) cards. The two DAQ cards were synchronized by the same clock signal (20 MHz). One DAQ card (DAQ1) also generated the driving waveforms, which were amplified before being sent to the PZT actuator (with a maximum drive amplitude to each electrode $\sim$75 V). The fiber tip sweep range was $\sim$500 μm, which corresponded to a beam-scanning range over the sample of $\sim$100 μm, given our miniaturized objective lens with an effective magnification $\sim$0.2 (from the fiber tip to the sample).

For the spiral scanning, the drive frequency f_R was $\sim$1,368 Hz (corresponding to a period of 730.8 μs), so the frame rate was $\sim$2.7 frames/second, with each frame consisting of 512 spiral scans. For the Lissajous scanning, the periods of the two sine waves were set to 731 μs and 730 μs, respectively. The repetition period of a complete scanning pattern was the least common multiple, i.e., $731 \times 730 = 533,630$ μs, corresponding to a frame rate $\sim$1.9 frames/second.

4 Results and Discussion

During imaging with either spiral or Lissajous scanning, signals from both detection channels were collected simultaneously, the raw data were saved with a time stamp, and the reconstructed images were displayed simultaneously. For the spiral scanning, we found that the membranes of the cells in the center ruptured about 4 min after illumination (and imaging) started. A representative series of TPF time-lapse images of the cells are shown in Fig. 4, with the continuous illumination time increasing from left to right. To differentiate the two fluorescence colors, pseudocolor is employed here, with green and red denoting fluorescence from SYBR-14 and PI, respectively.

At 4 min 20 sec after imaging started, the green signal from the cells (detected by the SYBR-14 fluorescence channel) in the scan center became very dim, and a fairly strong red signal began to appear at the same location in the PI fluorescence channel, which indicated the rupture of the cell membrane at about that time. Because SYBR-14 stains intact as well as ruptured cells, the dimming of SYBR-14 fluorescence is likely due to the overlap of its emission spectra with the excitation spectra
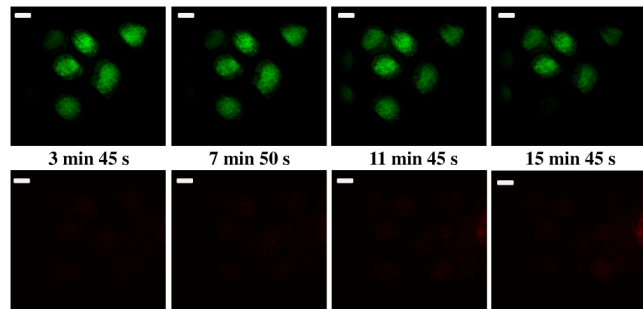
Fig. 5 A representative series of TPF images of cells collected by Lissajous scanning. Top row: SYBR-14 fluorescence images pseudocolored green. Bottom row: PI fluorescence images pseudocolored red. Images in the same column were collected at the same time, with the scanning time labeled in the middle of each column. The white scale bar represents 10 μm.

of PI. The off-center cells fluoresced only green throughout the imaging process, indicating that the cells remained alive with an intact membrane owing to the relatively low area illumination density shown in Fig. 2(c).

For Lissajous scanning, most cells within the field of view (FOV) stayed alive for more than 15 min. A representative series of TPF time-lapse images are shown in Fig. 5. One cell fluorescing green in the lower left corner of the FOV disappeared in the last frame (taken at 15 min 45 s). However, it should be noted that no red PI fluorescence signal from the same location was observed, suggesting that the disappearance of SYBR-14 fluorescence from that cell was not caused by cell death. One possible explanation is that that particular cell lost adherence to the coverslip after more than 15 min and floated out of focus. Similar arguments also applied to the appearance of dim PI fluorescence of one cell located on the right edge of the FOV. No green fluorescence (from SYBR-14) or change in green fluorescence was observed at the same location throughout the entire imaging period, suggesting that that cell might have died earlier and drifted from elsewhere into the FOV. Except for these two outliers, all other cells in the FOV maintained an almost constant SYBR-14 fluorescence intensity during the entire imaging period.

It should be noted that though the illumination density near the edges and corners of the Lissajous scanned region was relatively high according to our simulation, no visible photodamage to cells in those corresponding regions was observed in the experiments. One possible explanation is that the fiber tip, though slowing down, does not continuously linger around for a long time near the edges or corners of the scanned region. So, the cells in those regions only experienced relatively higher illumination power for a short period of time, which did not reach the level necessary to cause any visible photodamage.

5 Conclusion

In summary, we analyzed and compared the distribution of the TPF excitation light in the spiral and Lissajous scanning patterns, both theoretically and numerically. *In vitro* cell viability TPF imaging experiments were conducted, and the results confirmed our analyses. We found that more uniform illumination in the central region was achieved using Lissajous scanning. Unlike spiral scanning, where cells at the scan center experienced obvious photodamage, Lissajous scanning under the same

Fig. 4 A representative series of TPF images of cells collected by spiral scanning. Top row: SYBR-14 fluorescence images (shown in pseudo-green color). Bottom row: Propidium iodide (PI) fluorescence images (shown in pseudo-red color). Images in the same column were collected at the same time, with the scanning time labeled in the middle of each column. The scale bar represents 10 μm.

incident laser power did not cause visible photodamage over the entire scan region and over an even longer exposure time than in the case of spiral scanning. These results suggest that Lissajous scanning, which can be conveniently realized on a fiber-optic endomicroscope by an extremely compact tubular PZT actuator, provides a simple but effective solution to overcome the photo-damage issue associated with spiral scanning. This increases the feasibility of imaging cells or tissues over a long period of time, which is valuable for clinical diagnosis and basic biomedical research (such as for studying engineered tissue and cellular physiology). The stable and nearly rectangular FOV associated with Lissajous scanning also offers a more uniform pixel size over almost the entire scan area. In addition to TPF, the more uniform illumination scheme based on Lissajous scanning in an endoscope setting can also be very useful for other endoscopic nonlinear optical imaging (such as SHG imaging) and optical coherence tomography (OCT) imaging techniques.[8,16]

References

1. W. Denk, J. H. Strickler, and W. W. Webb, "Two-photon laser scanning fluorescence microscopy," *Science* **248**(4951), 73–76 (1990).
2. F. Helmchen et al., "A miniature head-mounted two-photon microscope: high-resolution brain imaging in freely moving animals," *Neuron* **31**(6), 903–912 (2001).
3. B. A. Flusberg et al., "In vivo brain imaging using a portable 3.9 gram two-photon fluorescence microendoscope," *Opt. Lett.* **30**(17), 2272–2274 (2005).
4. M. T. Myaing, D. J. MacDonald, and X. D. Li, "Fiber-optic scanning two-photon fluorescence endoscope," *Opt. Lett.* **31**(8), 1076–1078 (2006).
5. L. Fu et al., "Three-dimensional nonlinear optical endoscopy," *J. Biomed. Opt.* **12**(4), 040501-1–040501-3 (2007).
6. Y. C. Wu et al., "Scanning all-fiber-optic endomicroscopy systemfor 3D nonlinear optical imaging of biological tissues," *Opt. Express* **17**(10), 7907–7915 (2009).
7. Y. C. Wu et al., "Scanning fiber-optic nonlinear endomicroscopy with miniature aspherical compound lens and multimode fiber collector," *Opt. Lett.* **34**(7), 953–955 (2009).
8. X. M. Liu et al., "Rapid-scanning forward-imaging miniature endoscope for real-time optical coherence tomography," *Opt. Lett.* **29**(15), 1763–1765 (2004).
9. M. J. Cobb, X. M. Liu, and X. D. Li, "Continuous focus tracking for real-time optical coherence tomography," *Opt. Lett.* **30**(13), 1680–1682 (2005).
10. C. L. Hoy et al., "Miniaturized probe for femtosecond laser microsurgery and two-photon imaging," *Opt. Express* **16**(13), 9996–10005 (2008).
11. T.-M. Liu et al., "Miniaturized multiphoton microscope with a 24 Hz frame-rate," *Opt. Express* **16**(14), 10501–10506 (2008).
12. E. W. Weisstein, "Lissajous curve," *MathWorld—A Wolfram Web Resource*, http://mathworld.wolfram.com/LissajousCurve.html
13. D. L. Garner et al., "Dual DNA staining assessment of bovine sperm viability using SYBR-14 and propidium iodide," *J. Androl.* **15**(6), 620–629 (1994). http://www.andrologyjournal.org/cgi/content/abstract/15/6/620
14. Z. Zhang, "Cell viability and DNA denaturation measurements by two-photon fluorescence excitation in CW Al:GaAs diode laser optical traps," *J. Biomed. Opt.* **4**(2), 256–259 (1999).
15. Molecular Probes, "LIVE/DEAD Sperm Viability Kit," http://tools.invitrogen.com/content/sfs/manuals/mp07011.pdf (14 March 2001).
16. L. Huo et al., "Forward-viewing resonant fiber-optic scanning endoscope of appropriate scanning speed for 3D OCT imaging," *Opt. Express* **18**(14), 14375–14384 (2010).